Transverse spinning of particles in highly focused vector vortex beams

Manman Li,[1,2] Shaohui Yan,[1,*] Yansheng Liang,[1,2] Peng Zhang,[1] and Baoli Yao[1,†]

[1]*State Key Laboratory of Transient Optics and Photonics, Xi'an Institute of Optics and Precision Mechanics, Chinese Academy of Sciences, Xi'an 710119, People's Republic of China*

[2]*University of Chinese Academy of Sciences, Beijing 100049, People's Republic of China*

Transverse spin angular momentum, which appears locally in the structured optical fields, has attracted much attention, owing to its extraordinary properties and potential applications. We show theoretically that, by highly focusing a vector vortex beam with azimuthally varied polarization, it is possible to trap multiple particles simultaneously and manipulate the particles' spin along the azimuthal direction. Both the direction and the magnitude of the spin angular momentum, so the spin torque on the particle, can be varied by changing the state of the input beams. Moreover, the magnitude of the spin torque can be manipulated further by changing the characteristics of the particles. Such results may be exploited in practical optical manipulation, especially for optically induced rotations.

I. INTRODUCTION

The past decades have seen increasing attention in optical manipulation of microscopic objects since its unique advantages of noncontact and noninvasive operation capability [1,2]. One special but important class of optical manipulation is using optical torque to rotate a trapped particle [3]. This light-induced rotation is achieved from the shape asymmetry of a particle [4,5] or the transfer of optical angular momentum from light to the particle [6,7]. The angular momentum of light can be decomposed into two parts: the spin angular momentum (SAM) and the orbital angular momentum. The former is associated with the polarization of light, causing the rotation of a particle around its own axis, whereas the latter arises from the phase structure of light, resulting in the rotation of the particles around the optical beam axis [8]. In general, the axis of the induced rotation is parallel to the beam propagation axis [9–12]. Recently, the appearances of transverse SAM in various structured optical fields: evanescent waves, interference fields, and focused beams [13–15], make it possible to rotate the particle along a nonaxial direction [16–18]. This allows for additional rotation degrees of freedom in optical manipulation.

Polarization, as a fundamental and intrinsic property of light, plays an important role in light-matter interactions. The electromagnetic field, after focusing, is strongly polarization dependent, especially in the case of highly focused beams [19]. Compared to common optical beams with spatially uniform states of polarization (SOP), such as linear, circular, or elliptical polarizations, the beams with spatially inhomogeneous SOP, including spatially variant linear polarization [20,21] and hybrid SOP [22,23], have attracted immense interest due to their fascinating properties and novel applications in optical trapping [24], optical microscopy [25], quantum communication [26], nonlinear optics [27], etc. In addition, like the optical field itself, the SAM of the focused field is also polarization dependent. For instance, the tightly focused

field of an illumination with radial-variant hybrid polarization has been shown to induce orbital motion of isotropic particles [28,29]; a highly focused cylindrically polarized beam can exert a transverse spin torque on absorptive particles with the spin pointing between the radial and the azimuthal directions [30].

In this paper, we introduce a family of vector vortex beams with azimuthally varied SOPs and changeable polarization topological charge (PTC). We use the vectorical diffraction integral to represent the field distributions of these vector vortex beams focused by a high numerical aperture (NA) objective and then analyze the SAM of the focused fields. It is shown that the focused fields carry purely transverse SAM and can be used to induce azimuthal spinning on trapped particles. Effects of different parameters, such as the inner radius of the vector vortex beam, the sign and the value of the PTC, on the SAM and the spin torque are presented. Furthermore, the dependences of the spin torque on the particle's complex refractive index also are investigated.

II. THEORY

In optical trapping, the optical fields interacting with the target particle are actually the fields of some illumination focused by a high NA objective lens. According to the Richards-Wolf vectorial diffraction method [19,31], the focused electric field in the vicinity of the focus can be expressed in an integral as

$$\mathbf{E}(\mathbf{r}) = \frac{-ikf}{2\pi} \int_0^{\theta_{\max}} \int_0^{2\pi} \mathbf{A}(\theta,\phi) \exp\left(i\mathbf{k} \cdot \mathbf{r}\right) \sin\theta \, d\phi \, d\theta. \tag{1}$$

Here k is the wave number in the image space, and f is the focal length; $\theta_{\max}$ is the maximal converging angle determined by the NA; vectors $\mathbf{k}$ and $\mathbf{r}$ designate the wave vector and the observation point position in the image space, respectively; $\mathbf{A}(\theta,\phi)$ stands for the apodized field. The relationship between the apodized field $\mathbf{A}(\theta,\phi)$ and the input field $\mathbf{A}_0(\theta,\phi)$ at the entrance pupil is [32]

$$\mathbf{A}(\theta,\phi) = (\cos\,\theta)^{1/2} \begin{bmatrix} \mathbf{e}_\theta & 0 \\ 0 & \mathbf{e}_\phi \end{bmatrix} \begin{pmatrix} A_{0\rho} \\ A_{0\phi} \end{pmatrix}, \tag{2}$$

*shaohuiyan@opt.ac.cn

†yaobl@opt.ac.cn
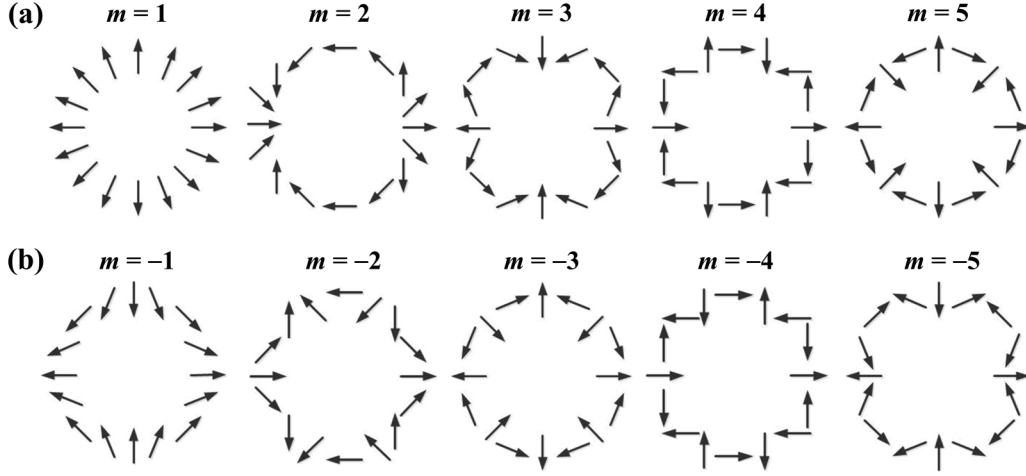
FIG. 1. Polarization distributions of incident vector vortex beams with (a) positive and (b) negative PTCs.

where $(\mathbf{e}_\theta, \mathbf{e}_\phi)$ are the respective unit vectors in the θ and ϕ directions and $(A_{0\rho}, A_{0\phi})$ are the radial and azimuthal components of the input field $\mathbf{A}_0(\theta, \phi)$. Here, we introduce a family of vector vortex beams with inhomogeneous linear polarization as

$$\mathbf{A}_0(\theta, \phi) = l(\theta)[\cos(m\phi)\mathbf{e}_x + \sin(m\phi)\mathbf{e}_y], \quad (3)$$

in which m is the PTC, just as shown in Fig. 1, that the polarization direction rotates $2\pi m$ counterclockwise around the beam axis in one circuit; $\mathbf{e}_x$ and $\mathbf{e}_y$ are the unit vectors in the x and y directions, respectively; $l(\theta)$ is the amplitude function assumed to have a simple form

$$l(\theta) = \begin{cases} l_0, & \sin^{-1}(\mathrm{NA}_1) \leqslant \theta \leqslant \sin^{-1}(\mathrm{NA}/n_1), \\ 0, & \text{otherwise,} \end{cases} \quad (4)$$

where l_0 is a constant factor dependent on the power of the incident field, n_1 denotes the refractive index of the image space, and NA_1 corresponds to the inner radius of the annulus, which is variable.

Integrating over the azimuthal direction in (1) yields the three field components (E_ρ, E_ϕ, E_z) in cylindrical coordinates (ρ_s, ϕ_s, z_s) as

$$E_\rho = Ci^{m-1}\cos[(m-1)\phi_s]\int_0^{\theta_{\max}}\cos^{1/2}\theta \, \sin \, \theta l(\theta)$$
$$\times e^{ikz_s\cos\theta}[(1+\cos\theta)J_m(\beta) + (1-\cos\theta)J_{m-2}(\beta)]$$
$$\times d\theta,$$

$$E_\phi = Ci^{m-1}\sin[(m-1)\phi_s]\int_0^{\theta_{\max}}\cos^{1/2}\theta \, \sin \, \theta l(\theta)$$
$$\times e^{ikz_s\cos\theta}[(1+\cos\theta)J_m(\beta) - (1-\cos\theta)J_{m-2}(\beta)]$$
$$\times d\theta,$$

$$E_z = 2Ci^m\cos[(m-1)\phi_s]\int_0^{\theta_{\max}}\cos^{1/2}\theta \, \sin^2\theta l(\theta)$$
$$\times e^{ikz_s\cos\theta}J_{m-1}(\beta)d\theta. \quad (5)$$

Here $\beta = k\rho_s\sin\theta$ and $C = kf/2$, $J_m(\beta)$ is the Bessel functions of the first kind of order m. The SAM density of the

focused fields is recognized as [33,34]

$$\langle \mathbf{S} \rangle = \frac{\varepsilon_0}{2\omega}\mathrm{Im}[\mathbf{E}^* \times \mathbf{E}], \quad (6)$$

where ε_0 is the permittivity of vacuum and ω is the angular frequency of light. From Eq. (5), it is observed that the transverse and longitudinal components of the focused fields are $\pi/2$ out of phase. In combination with Eq. (6), it clearly is seen that the longitudinal component of the SAM density vanishes and, therefore, the SAM density is purely transverse. A particle trapped in such focused fields is expected to undergo a spin transverse to the optical axis.

We now consider a Rayleigh spherical particle of permittivity ε_2 located in the focused fields given by Eq. (5). The medium in the image space surrounding the particle has permittivity ε_1. The particle has a radius a, being much smaller than the trapping wavelength so that the particle may be considered simply as an induced electric dipole. Then, the induced dipole moment is $\mathbf{p} = \alpha\mathbf{E}$, where α is the polarizability given by [35]

$$\alpha = \frac{\alpha_0}{1 - i(2/3)k^3\alpha_0}, \qquad \alpha_0 = 4\pi\varepsilon_1 a^3\frac{\varepsilon_2/\varepsilon_1 - 1}{\varepsilon_2/\varepsilon_1 + 2}. \quad (7)$$

The transfer of the linear momentum from light to the particle induces an optical force on the particle according to $\mathbf{F} = (\mathbf{p} \cdot \nabla)\mathbf{E} + (1/c)(\partial\mathbf{p}/\partial t) \times \mathbf{B}$, whereas the transfer of the angular momentum leads an optical torque given by $\mathbf{\Gamma} = \mathbf{p} \times \mathbf{E}$. As the external electric-field $\mathbf{E}$ varies harmonically in time, the time-averaged optical force and spin torque are [30]

$$\langle F_i \rangle = \frac{1}{2}\mathrm{Re}[\alpha E_j\partial_i(E_j)^*], \quad (8)$$

$$\langle \mathbf{\Gamma} \rangle = \frac{1}{2}|\alpha|^2\mathrm{Re}\left[\frac{1}{\alpha_0^*}\mathbf{E} \times \mathbf{E}^*\right]. \quad (9)$$

Here i, j denote the Cartesian components (x, y, z), the dummy index means a summation, and the symbol $*$ denotes the complex conjugate.

III. RESULTS AND DISCUSSIONS

We first analyze the intensity properties of the focused fields. Figure 2 shows the focal field intensity profiles for the
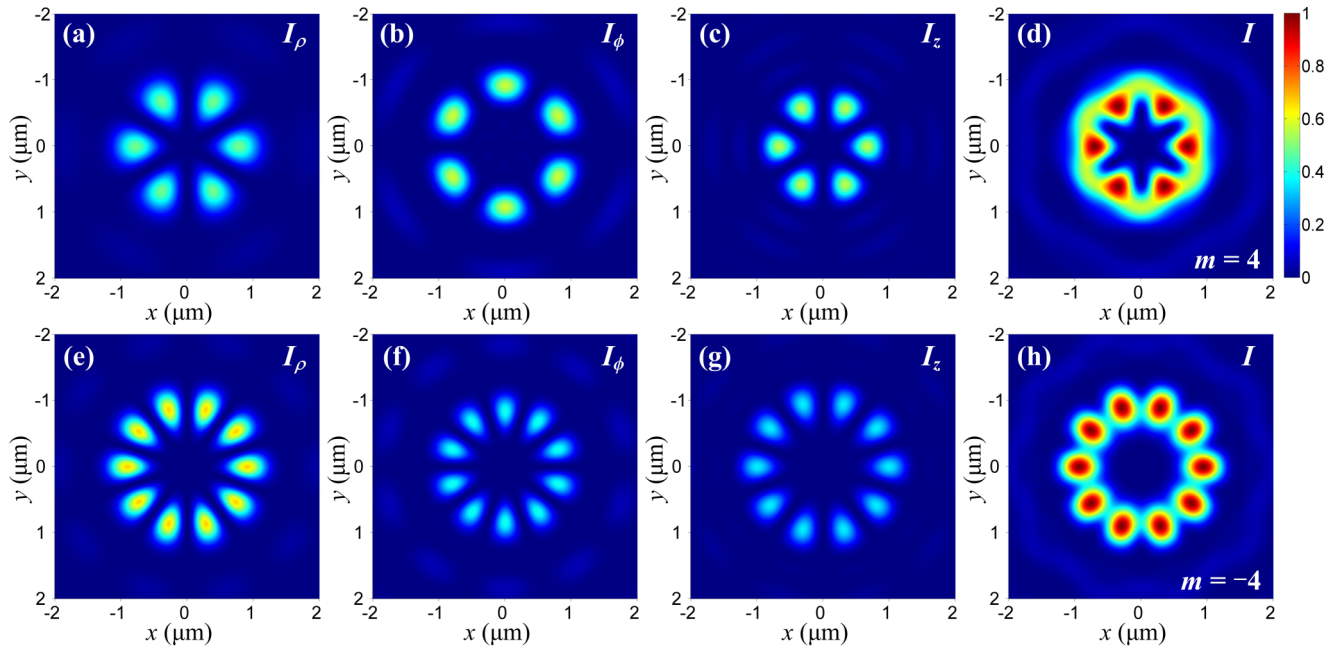
FIG. 2. Intensity distributions of highly focused vector vortex beams with respective PTCs (a)−(d) $m = 4$ and (e)−(h) $m = -4$.
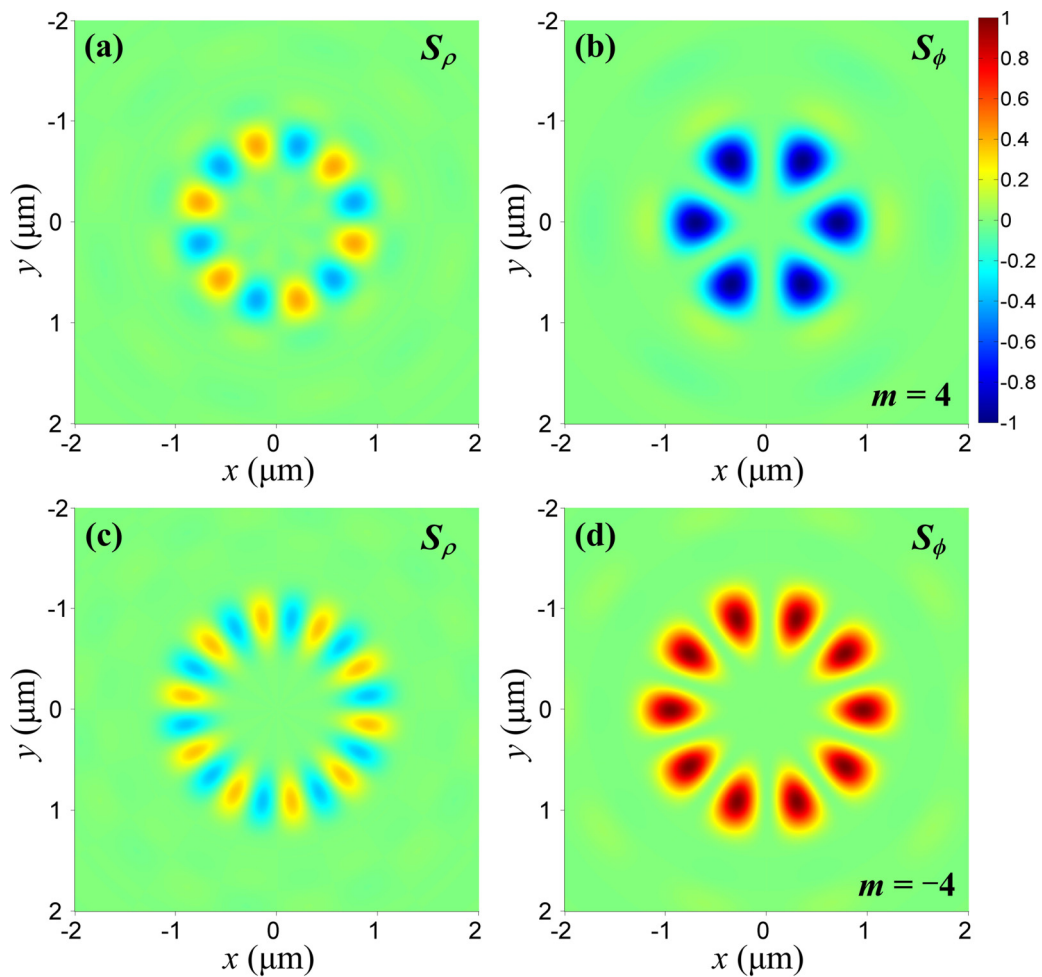
FIG. 3. Spin angular momentum density components in the focal plane for input beams with PTCs (a) and (b) $m = 4$ and (c) and (d) $m = -4$.

input beams with respective PTCs $m = 4$ and -4 focused by an objective lens of NA = 1.26 ($NA_1 = 0$). The incident wavelength is assumed to be $\lambda_0 = 1.064\,\mu m$, and the incident power is $P = 100\,mW$ throughout this paper. Shown in the upper (lower) row from left to right are the intensity components I_ρ, I_ϕ, and I_z as well as the total intensity I for $m = 4$ ($m = -4$). It is observed that all these intensities exhibit a ringlike pattern with $2|m - 1|$ lobes (petals) arranged symmetrically on the ring as shown in Figs. 2(a)–2(c) and 2(e)–2(g). This is a direct consequence of the azimuthal phase structure of the focused fields (5) in which the radial and longitudinal intensities have a $\cos^2[(m - 1)\phi_s]$ modulation whereas the azimuthal intensity varies as $\sin^2[(m - 1)\phi_s]$. Since I_ρ and I_z have more contributions than I_ϕ to the total intensity, the total intensity I varies approximately as $\cos^2[(m - 1)\phi_s]$ showing a petal-shaped pattern with $2|m - 1|$ hot spots as plotted in Figs. 2(d) and 2(h). Such intensity structures indicate a possible application for multiple-particle trapping.

In Fig. 3 we plot the normalized SAM densities of the focused fields in Fig. 2. As mentioned earlier, only transverse components S_ρ and S_ϕ occur. We see that the magnitudes of SAM densities also exhibit petal-shaped patterns and the radial component S_ρ has $4|m - 1|$ lobes along the azimuthal direction as shown in Figs. 3(a) and 3(c) whereas the azimuthal component S_ϕ has $2|m - 1|$ lobes as shown in Figs. 3(b) and 3(d). These lobelike structures in the magnitude of the SAM density arise directly from those contained in the focused fields (5). Furthermore, for either $m = 4$ or -4, the magnitude

of the radial component S_ρ is smaller than half that of the azimuthal component S_ϕ. In addition, S_ρ changes its sign alternately along the azimuthal direction, whereas S_ϕ is always negative or positive depending on the sign of PTC m.

The aforementioned discussion proves that the focused fields of vector vortex beams carry transverse optical SAM rather than conventional longitudinal SAM. We now examine their mechanical consequences when interacting with trapped particles. Consider a spherical Rayleigh particle of radius $a = 30\,nm$ with refractive index $n_2 = 1.59 + 0.005i$ ($\varepsilon_2 = \varepsilon_0 n_2^2$), suspended in water with refractive index $n_1 = 1.33$. Figure 4 shows the transverse optical forces and spin torques on the particle in the focal plane. It is seen that the particle can be trapped in each hot spot of intensity maximum as shown in Figs. 4(a) and 4(c) and will experience an azimuthal spinning motion as shown in Figs. 4(b) and 4(d). Here lies the fact that a particle in the equilibrium position experiences only the azimuthal SAM. With the PTC $m = 4$, the spinning is along the negative azimuthal direction, whereas for $m = -4$, the spinning reverses direction. Since the sign of the PTC determines the direction of the azimuthal SAM as shown in Figs. 3(b) and 3(d), the change in spinning orientation of the particle is self-explanatory.

We next turn our attention to the dependences of the azimuthal SAM density S_ϕ and the azimuthal spin torque Γ_ϕ on some parameters, such as the PTC, the inner radius of the annulus NA_1, and the refractive index of the particle. Figure 5(a) shows the changes in S_ϕ and Γ_ϕ evaluated at the
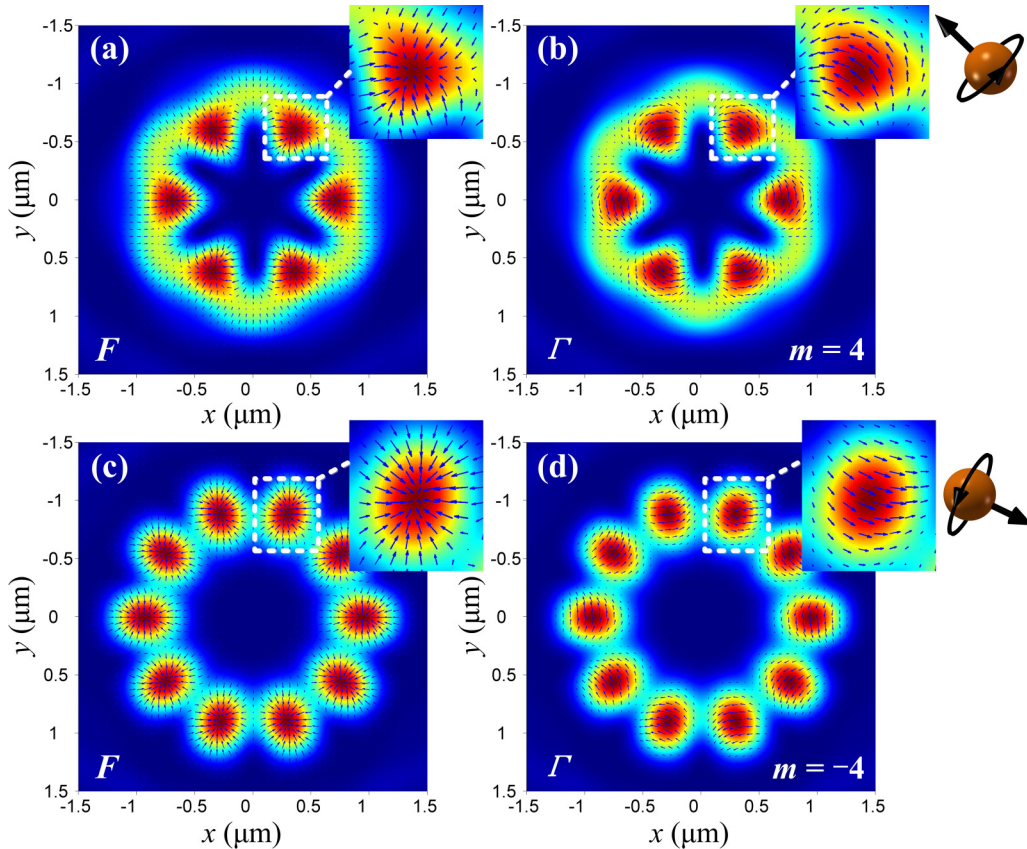
FIG. 4. Transverse force and spin torque distributions in the focal plane illuminated by vector vortex beams with PTCs (a) and (b) $m = 4$ and (c) and (d) $m = -4$.
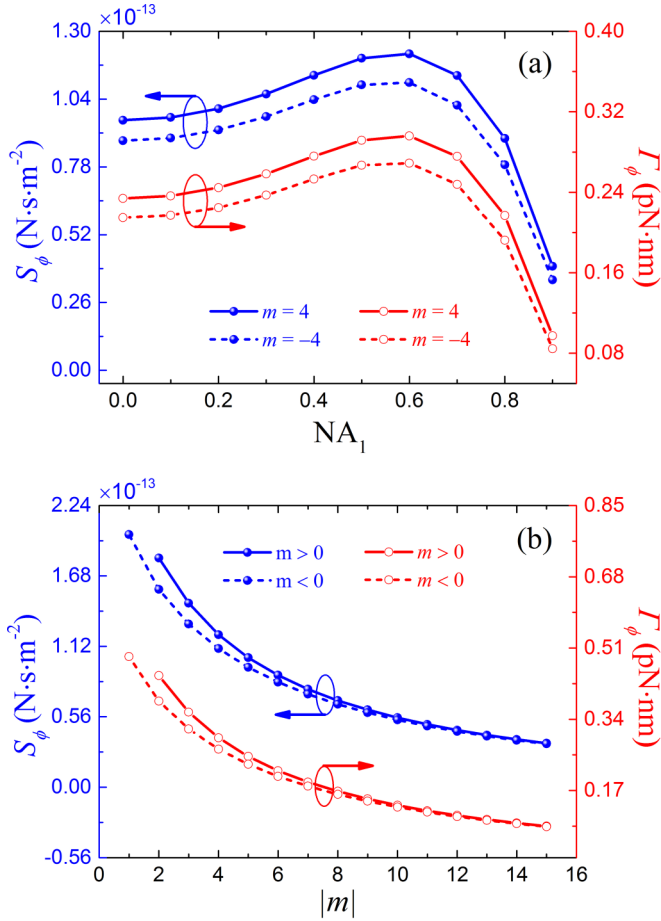
FIG. 5. Changes in the azimuthal spin angular momentum density and azimuthal spin torque in the equilibrium position with (a) the inner radius of the annulus NA_1 and (b) the PTC m.

equilibrium position as a function of NA_1 for PTCs $m = 4$ and -4, respectively. With increasing the value of NA_1, both S_ϕ and Γ_ϕ increase slowly until a peak is reached at $NA_1 = 0.6$, thereafter they decrease drastically. So, the inner radius takes this optimal value of 0.6 in the following calculations. The dependences of azimuthal SAM density and azimuthal spin torque on the PTC value of $|m|$ are shown in Fig. 5(b), where
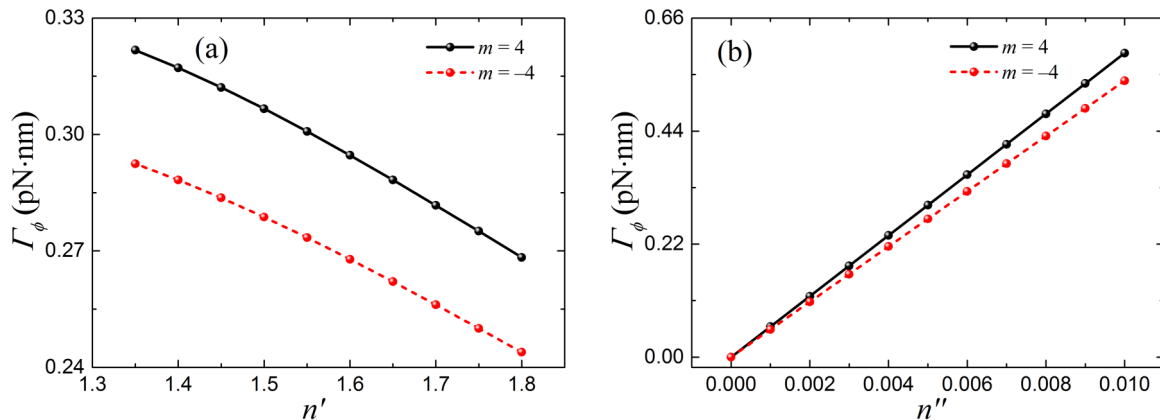
$m \leqslant -1$ or $m \geqslant 2$ since the case of $m = 1$ corresponds to radial polarization that carries no SAM in the focus. We see that both S_ϕ and Γ_ϕ decay with increasing the value of $|m|$, arising from the attenuation in the intensity of hot spots as the focusing ring expands with the increase in $|m|$. In addition, we observe that both the SAM density and the spin torque are larger for the case of $m > 0$ than for the case of $m < 0$. This can easily be understood by noting that, with the same magnitude of m, the case of $m > 0$ will yield a smaller focusing ring. In Fig. 5, it can be seen that the spin torque and the SAM density always show the same variation tendency, giving a direct verification that the mechanical spin torque on the particle comes from the transferred SAM from the light. More precisely, from the torque formula $\langle \boldsymbol{\Gamma} \rangle = (1/2)\mathrm{Re}[\alpha \mathbf{E} \times \mathbf{E}^*] = (1/2)\mathrm{Im}(\alpha)\mathrm{Im}(\mathbf{E}^* \times \mathbf{E}) = (\omega/\varepsilon_0)\mathrm{Im}(\alpha)\langle \mathbf{S} \rangle$, we see that the torque is proportional to the SAM density.

The dependence of the spin torque at the equilibrium position on the particle's complex refractive index $n_2 = n' + in''$ is investigated for the PTCs $m = 4$ and -4 in Fig. (6). In Fig. 6(a), we fix n'' at 0.005 and let n' vary, whereas in Fig. 6(b) n' is held at 1.59, and the imaginary part n'' varies. It is observed that the spin torque Γ_ϕ decreases with the increase in the value of the real part n', whereas it increases with increasing imaginary part n''. A straightforward examination of Eq. (9) shows that $\langle \Gamma \rangle \propto \mathrm{Im}(\alpha) \propto \mathrm{Im}\{[(n_2/n_1)^2 - 1]/[(n_2/n_1)^2 + 2]\}$ finding that $\langle \Gamma \rangle \propto 1/(n')^3$ for fixed n'' and $\langle \Gamma \rangle \propto n''$ for fixed n'. This demonstrates that the magnitude of the spin torque can be increased by decreasing the real part or increasing the imaginary part of the refractive index appropriately.

IV. CONCLUSIONS

To summarize, we investigated a method of manipulating particles to undergo a spin transverse to the optical axis. Tightly focused vector vortex beams exhibit petal-shaped intensity distributions and carry purely transverse SAM, which can be used to trap multiple particles simultaneously and spin particles along the azimuthal direction. The direction of the spinning motion can be changed by varying the sign of the polarization topological charge. When the charge is positive, the SAM is negative, and the spin torque vector points to the negative azimuthal direction; otherwise, the SAM and the

FIG. 6. Azimuthal spin torque on the particle with differing (a) real part n', and (b) imaginary part n'' of the refractive index at equilibrium position under vector vortex beams with PTCs $m = 4$ and -4.

spin torque vector reverse direction. Moreover, the size of the SAM and the spin torque can be controlled by adjusting the inner radius NA_1 and the polarization topological charge of the input beams with both quantities attaining a maximum value at $NA_1 = 0.6$ and decreasing with the charge increasing. We finally noted that the spin torque in magnitude can be increased further by properly decreasing the real part of the refractive index or increasing the particle's absorptivity. These results will assist in the investigation of optical manipulation, especially for optically induced rotation and transfer of optical SAM.

[1] D. G. Grier, A revolution in optical manipulation, Nature (London) **424**, 810 (2003).

[2] K. Dholakia and T. Čižmár, Shaping the future of manipulation, Nat. Photonics **5**, 335 (2011).

[3] D. L. Andrews, *Structured Light and Its Applications* (Academic, London, 2008), pp. 237–248.

[4] P. Jones, F. Palmisano, F. Bonaccorso, P. Gucciardi, G. Calogero, A. Ferrari, and O. Marago, Rotation detection in light-driven nanorotors, ACS Nano **3**, 3077 (2009).

[5] P. Galajda and P. Ormos, Complex micromachines produced and driven by light, Appl. Phys. Lett. **78**, 249 (2001).

[6] M. Friese, T. Nieminen, N. Heckenberg, and H. Rubinsztein-Dunlop, Optical alignment and spinning of laser-trapped microscopic particles, Nature (London) **394**, 348 (1998).

[7] L. Allen, M. W. Beijersbergen, R. Spreeuw, and J. Woerdman, Orbital angular momentum of light and the transformation of Laguerre-Gaussian laser modes, Phys. Rev. A **45**, 8185 (1992).

[8] M. Padgett and R. Bowman, Tweezers with a twist, Nat. Photonics **5**, 343 (2011).

[9] A. Lehmuskero, R. Ogier, T. Gschneidtner, P. Johansson, and M. Käll, Ultrafast spinning of gold nanoparticles in water using circularly polarized light, Nano Lett. **13**, 3129 (2013).

[10] Z. Yan and N. F. Scherer, Optical vortex induced rotation of silver nanowires, J. Phys. Chem. Lett. **4**, 2937 (2013).

[11] A. Lehmuskero, Y. Li, P. Johansson, and M. Käll, Plasmonic particles set into fast orbital motion by an optical vortex beam, Opt. Express **22**, 4349 (2014).

[12] R. Paez-Lopez, U. Ruiz, V. Arrizon, and R. Ramos-Garcia, Optical manipulation using optimal annular vortices, Opt. Lett. **41**, 4138 (2016).

[13] K. Y. Bliokh, A. Y. Bekshaev, and F. Nori, Extraordinary momentum and spin in evanescent waves, Nat. Commun. **5**, 3300 (2014).

[14] A. Y. Bekshaev, K. Y. Bliokh, and F. Nori, Transverse Spin and Momentum in Two-Wave Interference, Phys. Rev. X **5**, 011039 (2015).

[15] M. Neugebauer, T. Bauer, A. Aiello, and P. Banzer, Measuring the Transverse Spin Density of Light, Phys. Rev. Lett. **114**, 063901 (2015).

[16] A. Canaguier-Durand and C. Genet, Transverse spinning of a sphere in a plasmonic field, Phys. Rev. A **89**, 033841 (2014).

[17] K.-Y. Kim and S. Kim, Spinning of a submicron sphere by Airy beams, Opt. Lett. **41**, 135 (2016).

[18] M. Li, S. Yan, B. Yao, Y. Liang, and P. Zhang, Spinning and orbiting motion of particles in vortex beams with circular or radial polarizations, Opt. Express **24**, 20604 (2016).

[19] K. S. Youngworth and T. G. Brown, Focusing of high numerical aperture cylindrical-vector beams, Opt. Express **7**, 77 (2000).

[20] C. Maurer, A. Jesacher, S. Fürhapter, S. Bernet, and M. Ritsch-Marte, Tailoring of arbitrary optical vector beams, New J. Phys. **9**, 78 (2007).

[21] K. Huang, P. Shi, G. Cao, K. Li, X. Zhang, and Y. Li, Vector-vortex Bessel–Gauss beams and their tightly focusing properties, Opt. Lett. **36**, 888 (2011).

[22] G. M. Lerman, L. Stern, and U. Levy, Generation and tight focusing of hybridly polarized vector beams, Opt. Express **18**, 27650 (2010).

[23] B. Gu, Y. Pan, G. Rui, D. Xu, Q. Zhan, and Y. Cui, Polarization evolution characteristics of focused hybridly polarized vector fields, Appl. Phys. B: Lasers Opt. **117**, 915 (2014).

[24] H. Kawauchi, K. Yonezawa, Y. Kozawa, and S. Sato, Calculation of optical trapping forces on a dielectric sphere in the ray optics regime produced by a radially polarized laser beam, Opt. Lett. **32**, 1839 (2007).

[25] K. Lee, H. Kihm, J. Kihm, W. Choi, H. Kim, C. Ropers, D. Park, Y. Yoon, S. Choi, and D. Woo, Vector field microscopic imaging of light, Nat. Photonics **1**, 53 (2007).

[26] J. T. Barreiro, T.-C. Wei, and P. G. Kwiat, Remote Preparation of Single-Photon "hybrid" Entangled and Vector-Polarization States, Phys. Rev. Lett. **105**, 030407 (2010).

[27] A. Bouhelier, M. Beversluis, A. Hartschuh, and L. Novotny, Near-Field Second-Harmonic Generation Induced by Local Field Enhancement, Phys. Rev. Lett. **90**, 013903 (2003).

[28] X.-L. Wang, J. Chen, Y. Li, J. Ding, C.-S. Guo, and H.-T. Wang, Optical Orbital Angular Momentum from the Curl of Polarization, Phys. Rev. Lett. **105**, 253602 (2010).

[29] S. Yan, B. Yao, and M. Lei, Comment on Optical Orbital Angular Momentum from the Curl of Polarization, Phys. Rev. Lett. **106**, 189301 (2011).

[30] M. Li, S. Yan, B. Yao, M. Lei, Y. Yang, J. Min, and D. Dan, Intrinsic optical torque of cylindrical vector beams on Rayleigh absorptive spherical particles, J. Opt. Soc. Am. A **31**, 1710 (2014).

[31] B. Richards and E. Wolf, Electromagnetic diffraction in optical systems. II. Structure of the image field in an aplanatic system, Proc. R. Soc. London, Ser. A **253**, 358 (1959).

[32] Q. Zhan, Cylindrical vector beams: from mathematical concepts to applications, Adv. Opt. Photonics **1**, 1 (2009).

[33] F. Belinfante, On the current and the density of the electric charge, the energy, the linear momentum and the angular momentum of arbitrary fields, Physica **7**, 449 (1940).

[34] M. V. Berry, Optical currents, J. Opt. A: Pure Appl. Opt. **11**, 094001 (2009).

[35] B. T. Draine, The discrete-dipole approximation and its application to interstellar graphite grains, Astrophys. J. **333**, 848 (1988).